Coating gold nanorods with self-assembling peptide amphiphiles promotes stability and facilitates in vivo two-photon imaging

Egorova, E.A.; Arias Alpizar, G.; Vlieg, R.C.; Gooris, G.S.; Bouwstra, J.A.; Noort, S.J.T. van; ... ; Boyle, A.L.

Journal of Materials Chemistry B

ROYAL SOCIETY OF CHEMISTRY

PAPER

View Article Online
View Journal | View Issue

Cite this: *J. Mater. Chem. B*, 2022, **10**, 1612

Coating gold nanorods with self-assembling peptide amphiphiles promotes stability and facilitates *in vivo* two-photon imaging†

Elena A. Egorova, ‡[a] Gabriela Arias-Alpizar,§[ab] Redmar C. Vlieg,§[c] Gert S. Gooris,[b] Joke A. Bouwstra,[b] John van Noort,[c] Alexander Kros *[a] and Aimee L. Boyle *[d]

Received 11th January 2022,
Accepted 8th February 2022

DOI: 10.1039/d2tb00073c

rsc.li/materials-b

Gold nanorods (GNRs) are versatile asymmetric nanoparticles with unique optical properties. These properties make GNRs ideal agents for applications such as photothermal cancer therapy, biosensing, and *in vivo* imaging. However, as-synthesised GNRs need to be modified with a biocompatible stabilising coating in order to be employed in these fields as the ligands used to stabilise GNRs during synthesis are toxic. An issue is that GNR performance in the aforementioned techniques can be affected by these modified coatings. For example if coatings are too thick then GNR entry into cells, or their sensitivity in sensing applications, can be compromised. Here we show that thiolated peptide amphiphiles (PAs) can act as GNR stabilisers and provide a thin and highly-stable coating under physiologically relevant conditions. Additionally, all tested PAs formed highly ordered (51.8–58.8% β-content), and dense (2.62–3.87 peptides per nm^2) monolayers on the GNR surface. Moreover, the PA-coated GNRs demonstrated no cytotoxicity *in vitro* and, *via* injection in zebrafish embryos, the behavior and cellular interactions of such PA-coated GNRs were visualised *in vivo*, in real time, with two-photon (2P) microscopy.

Introduction

Gold nanorods (GNRs) are asymmetric nanoparticles whose physical dimensions and optical properties are tunable.[1–4] The GNR aspect ratio (a.r.), which is the relationship between its length and width, defines its optical properties as the a.r. affects the position of the longitudinal surface plasmon resonance (LSPR) band. The position of the LSPR can vary between 600 nm and 1200 nm. Due to the fact that the LSPR position is in the near-infrared (NIR) region of the electromagnetic spectrum, outside the region where water and biological molecules absorb, GNRs are considered to be suitable for a range of biomedical applications. For example, the absorption coefficient of GNRs is increased by several orders of magnitude upon irradiation with a laser whose wavelength matches their LSPR. This phenomenon has enabled GNRs to be employed as extraordinarily bright substrates for *in vitro* and *in vivo* two-photon (2P) luminescence imaging,[5–9] photothermal therapy,[10] and biosensing.[11]

An issue with as-synthesised GNRs is that they are unstable under physiological conditions, which affects their optical properties, causes significant cytotoxicity, and limits their use in biomedical applications.[12] The reason for this instability is the presence of cationic surfactants such as cetyltrimethylammonium bromide (CTAB),[13] cetyltrimethylammonium chloride (CTAC),[14] benzyldimethylhexadecylammonium chloride (BDAC), or mixtures thereof,[3] on the surface of as-synthesized GNRs. These molecules, together with silver nitrate ($AgNO_3$), allow for shape and size control during synthesis, and also act as GNR stabilisers. Several methods have been developed to displace these surfactants from the GNR surface, *e.g.* by using thiolated polyethylene glycol (PEG) molecules,[15,16] polyelectrolytes,[17,18] silica condensation,[19] or replacement of CTAB with its thiolated analogues.[20,21] These methods create a steric barrier between individual GNRs, minimising aggregation, whilst thiolated PEGs form a shell on the gold surface through the formation of Au–S bonds. These coatings have facilitated the use of GNRs in a range of biological applications.[9,10,22]

When coating GNRs to improve their stability, coating thickness should also be considered as this is important for many applications. For example, for ligand–receptor interactions

[a] *Department of Supramolecular & Biomaterials Chemistry, Leiden Institute of Chemistry, Leiden University, Leiden, The Netherlands. E-mail: a.kros@chem.leidenuniv.nl*
[b] *Division of BioTherapeutics, Leiden Academic Centre for Drug Research, Leiden University, Leiden, The Netherlands*
[c] *Leiden Institute of Physics, Leiden University, Leiden, The Netherlands*
[d] *Department of Macromolecular Biochemistry, Leiden Institute of Chemistry, Leiden University, Leiden, The Netherlands. E-mail: a.l.boyle@chem.leidenuniv.nl*

† Electronic supplementary information (ESI) available. See DOI: 10.1039/d2tb00073c

‡ Current address: Elena A. Egorova, Sirius University, Sochi, Russia.
§ Gabriela Arias-Alpizar and Redmar C. Vlieg contributed equally.

the studied interaction should take place as close to the gold surface as possible because the LSPR is defined by the local refractive index close to the particle surface.[23] The shift of the LSPR band is therefore a direct measure of the studied interactions and is affected by the coating thickness.[23,24] For *in vivo* applications, GNRs have to be delivered to their intended target and larger particles are not transported as effectively.[25–27] In such cases PEGylation, which is the most widely-used GNR stabiliser, might not be optimal. Whilst thiolated PEGs of 5–10 kDa are widely employed for GNR stabilisation,[15] this PEG size corresponds to a contour length of >30 nm for a fully "stretched" molecule.[28,29] Silica coatings are also typically >10 nm thick.[30] Such coatings therefore significantly enhance the dimensions of the GNRs. In addition, these molecules do not provide a facile route to further functionalisation with targeting ligands or therapeutic agents.

An ideal GNR coating would therefore be one that is thin, effective at stabilising the particle, and amenable to functionalisation. We have previously demonstrated that spherical gold nanoparticles (GNPs) can be stabilised by peptide amphiphiles (PAs).[31] These amphiphilic molecules are small (≈ 5 nm contour length) and consist of one or two thiolated alkyl chains and a peptide domain. The alkyl chains bind the gold surface *via* Au–S bonds and create a hydrophobic environment around the GNP core, while the charged peptide domains provide electrostatic repulsion between individual particles. The peptide portion also promotes self-assembly at the GNP surface which contributes to the overall stability. Additionally, the peptide is amenable to further derivatisation. Moreover, PAs are not recognised by the immune system,[32] while it has been reported that repeated administration of PEG induces specific immune responses.[33] Therefore, we propose that PAs could serve as stabilising coatings for GNRs.

In this study, PAs were evaluated together with thiolated PEG molecules to investigate whether PAs can provide a comparable, or improved, level of stabilisation. To facilitate PA coating, a ligand exchange procedure was developed to replace the original CTAB bilayer on the GNR surface with PA molecules varying in hydrophobicity and charge. These GNR conjugates were investigated using UV-Vis spectroscopy, transmission electron microscopy (TEM) imaging, and Fourier-transform infrared spectroscopy (FT-IR) to determine their aggregation tendency, coating thickness and peptide secondary structure. The stability of the PA-coated GNRs at high salt concentrations and in the presence of competing thiols was also tested. Finally, we demonstrate the *in vivo* potential of these particles by combining intravenous administration in zebrafish embryos with 2P microscopy. This strategy allows visualisation of GNRs in circulation and the identification of cellular interactions, indicating their suitability for use in biomedical applications.

Experimental

General

All chemicals were purchased from Sigma-Aldrich unless stated otherwise. Silver nitrate and Oxyma Pure were purchased from Carl Roth GmbH. TFA, piperidine, DMF, DCM, methanol, and acetonitrile were purchased from Biosolve. Fmoc- amino acids were purchased from Novabiochem. Thiolated PEG molecules ($HS–PEG–OCH_3$ with average MWs of 750 Da and 5000 Da) were supplied by Rapp Polymere GmBH. TEM grids (Formvar/carbon, 200 mesh, on copper support) were purchased from Electron Microscopy Sciences. The LDH assay kit was purchased from BioLegend.

Gold nanorod synthesis

GNRs were synthesised in a two-step process commonly described as a seed-mediated approach.[3] 2–3 nm seeds were prepared by mixing CTAB (5 mL, 0.20 M), and $HAuCl_4$ (5 mL, 0.50 mM) with ice-cold $NaBH_4$ (0.60 mL, 10 mM) whilst intensely stirring at room temperature.[34] After 2 min, the solution was left undisturbed at room temperature for 2 hours. For the overgrowth, solutions of $HAuCl_4$ (50 mL, 1.0 mM) and $AgNO_3$ (200 μL, 100 mM) were gently mixed with CTAB (50 mL, 0.20 M) at room temperature. After 2 min of stirring, ascorbic acid (550 μL, 100 mM) was added. Next, 120 μL of the seed solution was added under vigorous stirring. After 6 hours the rods were washed with MilliQ water (2×100 mL) and centrifuged to remove the excess CTAB. Average GNR dimensions were found to be 46.4×14.0 nm.

PA and peptide synthesis

All PAs and the peptide were synthesised by solid-phase peptide synthesis using standard Fmoc-chemistry protocols. The synthesis was performed on an automated Liberty Blue microwave peptide synthesizer (CEM). 20% piperidine in dimethylformamide (DMF) was used as the deprotection agent and *N*,*N*′-diisopropylcarbodiimide (DIC)/Oxyma Pure were employed as the activator/activator base. All sequences were synthesised on a Wang resin preloaded with either a glutamate or glycine residue (**1**, **2**, **3**, **4**, **1-W**, **2-W**, **3-W**) or a Rink Amide resin (**1-K** and **2-K**). The alkyl chain was coupled on resin to the terminal amine of the corresponding peptide using the same protocol as for amino acid coupling. The terminal thiol of the alkyl chains was subsequently manually blocked with 2,2′-dithiobis(5-nitropyridine) (DTNP, 1 eq. in DMF, RT, 3 hours). All molecules were cleaved from the resin using trifluoroacetic acid (TFA) with 1.5% deionized water, 2.5% triisopropylsilane (TIS), and in the case of **4**, 2.5% 3,4-ethylenedioxythiophene (EDOT). The crude molecules were precipitated into cold diethyl ether, pelleted by centrifugation, redissolved in water, and lyophilised prior to purification.

PA and peptide purification

A Shimadzu HPLC system equipped with two LC-20AR pumps, an SPD-20A UV-Vis detector, and a Phenomenex Kinetex EVO C18 column (21.2 by 150 mm) was used for purification. The mobile phases were water and acetonitrile (MeCN), containing either 0.1% ammonia (for **1–3** and **1-W**, **2-W**, **3-W**) or 0.1% TFA (for **4**, **1-K**, and **2-K**). Prior to purification of **1–3**, the protecting TNP group was removed by incubation with tris(2-carboxyethyl) phosphine hydrochloride (TCEP, added in excess, 30 min). The purity of the compounds was assessed using LC-MS (Fig. S1–S9, ESI†).

All purified molecules were lyophilised and stored at −20 °C until needed.

Coating GNRs with thiolated PAs

GNRs were coated using a ligand exchange approach. The ligand (*i.e.* the PA) was dissolved in DMSO and GNRs were added. The ligand excess was at least 100 000-fold (mol) relative to the GNR concentration.[34] The two components were mixed in such a ratio to ensure that the final concentration of DMSO in the mixture was 50% (v/v) for **GNR@1**, **GNR@2**, and **GNR@3**, or 10% (v/v) for **GNR@4**, **GNR@1-K**, and **GNR@2-K**. After incubation (1 hour for **1–4**; 16 hours for **1-K** and **2-K**) the samples were centrifuged, the supernatant was replaced with 25% DMSO (aq.) (**GNR@1**, **GNR@2**, and **GNR@3**) or 5% DMSO (aq.) (**GNR@4**, **GNR@1-K**, and **GNR@2-K**). **GNR@1-K** and **GNR@2-K** were directly loaded onto a size exclusion chromatography column (SEC, NAP-25 columns, GE Healthcare) to remove any remaining free ligand and to exchange the solvent for MilliQ water. The **GNR@1**, **GNR@2**, and **GNR@3** samples were incubated in 25% DMSO overnight to solubilise unbound PAs. After centrifugation, the GNRs were resuspended in 5% DMSO (v/v) and SEC purification was performed in phosphate buffered saline (PBS, pH 7.2).

PEGylation of GNRs

Thiolated PEGs were dissolved in DMSO (10 mg mL^{-1}). The PEG excess was at least 100 000-fold relative to GNR molar concentration. The PEG solution and GNR suspension were mixed, resulting in a final concentration of 10% (v/v) DMSO. The mixture was left overnight before excess PEG was removed *via* centrifugation (14 000 rpm, 15 min). GNRs were resuspended in MilliQ water and directly purified by SEC with PBS as the eluent.

UV-Vis spectroscopy

Spectra were recorded using a Cary 300 UV-Vis spectrophotometer. Samples were placed in 10 mm quartz cuvettes and spectra were recorded between 900–350 nm unless otherwise stated. Samples were diluted with either water or PBS as appropriate to provide a maximum absorbance in the range of 0.6–1.0. All spectra were normalised to a maximum absorbance of 1.0, except for the induced aggregation experiments where spectra were not normalised and aggregation factors were calculated as described below.

For GNRs with an a.r. of 3.3, $\varepsilon_{LSPR}(GNR) = 4.6 \times 10^9$ M^{-1} cm^{-1} was used.[34] For tryptophan absorbance $\varepsilon_{280}(W) = 5600$ M^{-1} cm^{-1} was used.

Transmission electron microscopy

A 10 μL GNR sample droplet was placed on a continuous carbon grid and left undisturbed for 10 min. The excess sample was removed by manually blotting with a fibreless paper tissue. A water droplet (10 μL) was put on the grid to wash off the unbound sample and blotted immediately. Uranyl acetate stain (0.5% w/v, 10 μL) was applied, followed and blotted after 10 s. Images were acquired on a JEM1400 Plus (JEOL) transmission electron microscope operated at 80 kV, equipped with a CCD camera.

Zeta potential measurements

A Zetasizer Nano-7 S (Malvern Instruments) equipped with a 633 nm wavelength laser and a 173°-fixed scattering angle was used to perform zeta potential measurements. Samples in PBS were diluted 10 times with deionized water to obtain a salt concentration below 20 mM. Sample aliquots of 1 mL were placed in a universal dip cuvette and the zeta potential was calculated from an average of three measurements.

Coverage density measurements

Coverage densities were determined through measuring the unbound ligand concentration.[31,35] Three PAs were extended with a Trp coupled *via* a glycine spacer to yield **1-W**, **2-W**, **3-W** (Fig. S10, ESI†). Tryptophan-tagged molecules **1-W**, **2-W**, and **3-W** were dissolved in HFIP and mixed with CTAB-protected GNRs yielding a final HFIP concentration of 33% (v/v). After a 1 hour incubation, the samples were centrifuged and the supernatant collected. The GNR pellets were resuspended in water and lyophilised. Next, GNRs were resuspended in HFIP and pelleted again. The PA concentration in both supernatants was determined by measuring the absorbance at 280 nm using UV-Vis ($\varepsilon_{280}(W) = 5600$ M^{-1} cm^{-1}). Since the concentration of **1-W**, **2-W**, and **3-W** added to the GNR suspension was known, the concentration of the unbound ligands in the combined supernatants was calculated, and from this the number of bound ligands was determined. The number of ligands per particle was subsequently calculated by dividing the concentration of bound ligands by the molar concentration of the GNRs.[34] The coverage density expressed in peptide per nm^2 was derived from the average surface area of a rod (2041 nm^2).

Infra-red spectroscopy measurements

Attenuated total reflection-infrared (ATR-IR) spectra were recorded on an Excalibur FTS 4000 setup equipped with a ''golden gate'' accessory. For each measurement, a background (air) was taken from the Golden Gate diamond after careful cleaning. Coated GNRs were desalted using a SEC column, lyophilised, and then resuspended in a drop of D_2O. A sample was placed on top of the crystal and left to dry. Spectra were recorded using the following settings: 512 scans at 2 cm^{-1} aperture. Deconvolution and fitting of the Amide I peaks to the Lorenz function were performed using Origin Pro. Surface areas under the individual peaks were measured to determine the distribution of different peptide secondary structure types. Amide I spectra for non GNR-bound PAs **1–3** and their secondary structure profiles (>85% β-content) can be found in our previous work.[31]

Evaluation of GNR stability at different ionic strengths

GNRs coated with **1–3**, thio-PEG5000, and thio-PEG750 were mixed with a 4.5 M NaCl solution to yield samples with the following final concentrations of salt: 150 mM, 500 mM, 1.5 M and 3.0 M. For GNRs coated with **1-K** and **2-K** the following

concentration range was used: 10, 50, 100, 150, and 500 mM NaCl. The GNR concentration remained constant (the peak maximum of the LSPR, OD_{LSPR} = 0.2–0.4) while only the salt concentration was varied. A spectrum from 500–800 nm was recorded using an Infinite M1000 plate-reader (Tecan). The OD_{LSPR} of each sample was compared to that of a GNR suspension with no salt added (0 mM NaCl). When GNRs aggregate, they exhibit a red-shift and often a broadening of the plasmon band. The OD of the samples with increasing amounts of NaCl was monitored and a decrease in the OD_{LSPR} value indicated aggregation.

Stability to DTT-competition

A DL-dithiothreitol (DTT) competition assay was used to assess permeability of the PA shells formed around the GNRs. The protocol used in this study was a modification of that published by the Mattoussi group.[36] Briefly, 4 M DTT, deionized water and the coated GNRs were mixed so that the final concentration of DTT was 1 M. The OD_{LSPR} value was monitored by UV-Vis for 90 min with a 5 min interval between the data points to assess the aggregation state. The OD_{LSPR} at the 0 min time point was maintained within a range of 0.5–0.9 for all GNR samples. The ratio between the OD at 610 nm and OD_{LSPR} gave rise to the aggregation factor (AF), which was normalized to the value at t = 0 min.

LDH release assay

Murine bone-marrow dendritic cells were a kind gift of Dr. B. Slütter, LADCR division of Leiden University. The assay was performed according to the manufacturer's manual. Briefly, 20×10^3 cells were plated in 96-well plates and then coated GNRs were added to the cells (50 μL per well, 200 μL total volume). PBS was used as negative control, while the assay lysis buffer was used as positive control. After 24 h, 30 μL of the cell culture medium were taken for the analysis and mixed with the assay substrate according to the manual. The percentage of observed cytotoxicity reflects the difference between the studied samples, PBS (0% cytotoxicity) and lysis buffer (100% cytotoxicity). Each GNR sample was tested in triplicate as well as at three concentrations (0.03, 0.11, 0.43 nM). Statistical analysis was performed using GraphPad Prism 9.

Zebrafish husbandry and intravenous injections

Zebrafish (*Danio rerio*, strain AB/TL) were treated in accordance with the European Convention guidelines on the protection of vertebrate animals in experimental and other scientific interests,[37] as well as the directives developed by the animal welfare committee of Leiden University. Fertilisation *via* natural spawning was conducted at the beginning of the light period, and eggs were maintained at 28.5 °C in egg water (60 μg mL^{-1} Instant Ocean sea salts). Prior injection, the embryos were embedded in 0.4% agarose containing 0.01% tricaine for anaesthesia. **GNR@3** were injected into 2 day old zebrafish embryos (54–56 hpf) using a modified microangraphy protocol.[38] A sample volume of 1 nL was calibrated and injected into the embryo's sinus venosus/duct of Cuvier. Further information on the injection procedure, is reported in ref. 39 and 40.

Two-photon setup and zebrafish imaging

Two wt zebrafish embryos injected with **GNR@3** were selected for two-photon *in vivo* microscopy imaging. The embryos were embedded in agarose gel and placed on a glass coverslip. The imaging was performed starting from 1 hour post injection using a custom-built two-photon multifocal microscope.[39] The excitation source, a femtosecond pulsed Ti:Sa laser was set at 800 nm during the imaging process (Coherent, Chameleon Ultra). A diffractive optical element (DOE, custom made by Holoeye) was used to achieve multifocal illumination of the sample (splitting of the laser beam into an array of 25 × 25 foci). Spiral scanning the foci within the 50 ms exposure time of the camera using a fast-scanning mirror (Newport, FSM-300-1) was used to create a virtual light sheet. The emission photons collected by a 25×, high-NA water-dipping objective (Nikon, CFI75 Apochromat 25XC W), positioned onto a piezo stage (P-726 PIFOC, PI) allowing for z-stack measurements. A dichroic mirror (700 dcxr, Chroma) was used to separate the emission light from the excitation path. To detect emission photons, the setup was equipped with a 2048 × 2048 pixels CMOS camera (Hamamatsu, Orca Flash 4.0 V2). Two-photon microscopy data was processed using custom-built LabVIEW software (version 2018 SP2, National Instruments). Images were analysed using the Fiji distribution of ImageJ.

Results and discussion

Coating of GNRs with PAs of different charges

PAs comprising a thiolated alkyl chain of either 16 or 11 carbons in length and a peptide domain with the sequence $V_3A_3X_3$ were synthesised (X = E/K, molecules **1**, **2**, **1-K**, and **2-K** in Scheme 1).[31] This approach facilitated the study of the effect of charge on the GNR stabilising capacity, as E (glutamic acid) gave rise to negatively charged PAs, and K (lysine) – to positively charged PAs. The construct with two C11 alkyl chains, molecule **3**, was introduced to probe the effect of a bidentate binding ligand. The sequence of **3** was extended with a fourth glutamic acid residue for increased solubility. Peptide **4** contained a cysteine (Cys, C) amino acid instead of a thiolated alkyl chain and served as a reference molecule to study the impact of the hydrophobic alkyl chain domain.

In addition to using molecule **4** as a reference, GNRs were also coated with thiolated PEG–OMe with average molecular weights of 750 and 5000 Da. Thiolated PEG5000 has been reported to be of an optimal length for GNR stabilisation, while thiolated PEG750 was chosen because its contour length in its extended conformation, (4.8 nm based on 0.28 nm per $-CH_2CH_2O-$ repeat),[28,29] is comparable to the length of the PAs used in this study.

GNRs with an a.r. of 3.3, giving rise to an LSPR band at 756 nm were synthesised according to the seed-mediated overgrowth method.[3,34] The average dimensions of the resulting

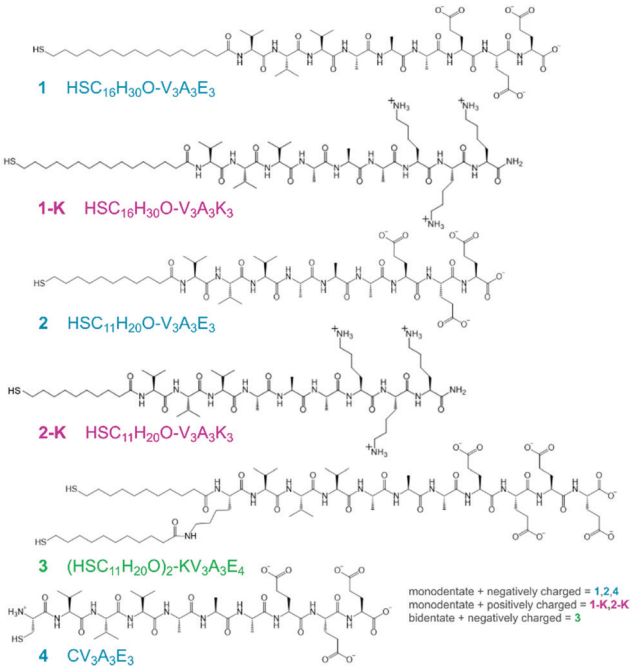

Scheme 1 Sequences and structures of PAs and peptides used in this study.

rods were 46.4 (±8.3) by 14.0 (±2.9) nm. Rods with these dimensions were selected as they are optimal for 2P microscopy.[24] As-synthesized GNRs were stabilised with cetyltrimethylammonium bromide (CTAB) which was displaced from the GNR surface *via* ligand exchange with the thiol-containing PAs/peptide and thiolated PEGs (750 and 5000 Da). Size-exclusion chromatography (SEC) was used to remove excess ligand and to concomitantly replace the medium with the buffer of choice.

The devised coating procedure resulted predominantly in non-aggregated GNR samples, as determined by UV-Vis spectroscopy (Fig. 1) and TEM analysis (Fig. 2). For all molecules apart from **4**, no apparent broadening of the LSPR band occurred, and only a moderate red-shift (7–10 nm) was detected, indicative of a change in the refractive index at the GNR surface upon CTAB exchange.[24] However, a larger red-shift (+16 nm), as well as some peak broadening was observed for **GNR@2-K**. Nevertheless, TEM imaging revealed no aggregation for this sample (Fig. 2H). Shells formed by the PAs around the GNRs were observed with TEM due to accumulation of the uranyl acetate stain. The thicknesses of these shells are likely to represent a collapsed PA monolayer at the GNR surface, since the shell was measured to be <2 nm thick in all cases.

Molecule **4** failed to prevent GNRs from aggregating. Due to a high amount of aggregation occurring during the coating procedure, this sample was not SEC-purified. TEM imaging revealed limited shell formation around **GNR@4**, (Fig. 2D). The evident loss of the plasmon band in the UV-Vis spectra and the presence of large **GNR@4** aggregates as visualised by TEM suggested that unlike spherical GNPs, GNRs cannot be stabilised by a simple peptide, likely due to its hydrophilicity. Therefore, the presence of the N-terminal alkyl chain indeed facilitated effective surface modification of GNRs, as has been previously reported.[16]

PEGylation of GNRs resulted in broadening of the LSPR band for **GNR@PEG750**, indicative of aggregation, while **GNR@PEG5000** showed a red-shift (+11 nm) but no peak broadening, consistent with previous reports (Fig. 1A).[15] TEM imaging showed that **GNR@PEG5000** indeed consisted of well-dispersed single GNRs, whilst **GNR@PEG750** formed small, compact aggregates (Fig. 2E and F). The PEG shells could not be visualised, most likely due to their low density and poor electron contrast.

As additional evidence for the successful displacement of CTAB from the GNR surface, the zeta-potential of GNRs before and after modification was measured. In contrast to **GNR@CTAB** (+36.6 mV), GNRs coated with the negatively charged PAs yielded negative zeta-potential values (−27.3 mV for **GNR@1**, −21.1 mV for **GNR@2**, and −20.7 mV for **GNR@3**, Fig. S15, ESI†). PA-coated spherical GNPs have previously shown zeta-potential values in the same range.[31] PEGylation

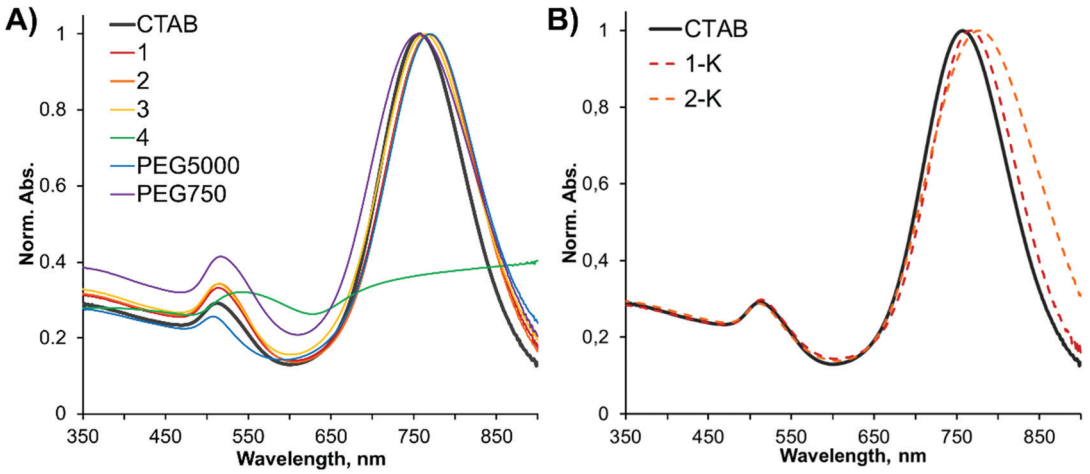

Fig. 1 UV-Vis spectra of GNRs before (CTAB) and after surface stabilisation with: (A) negatively charged PAs **1–3** and peptide 4, and (B) positively charged PAs **1-K** and **2-K**. Thiolated PEGs (750 and 5000 Da) were used as a reference stabiliser. Samples were prepared in (A) PBS (pH 7.2) or (B) in MilliQ water.

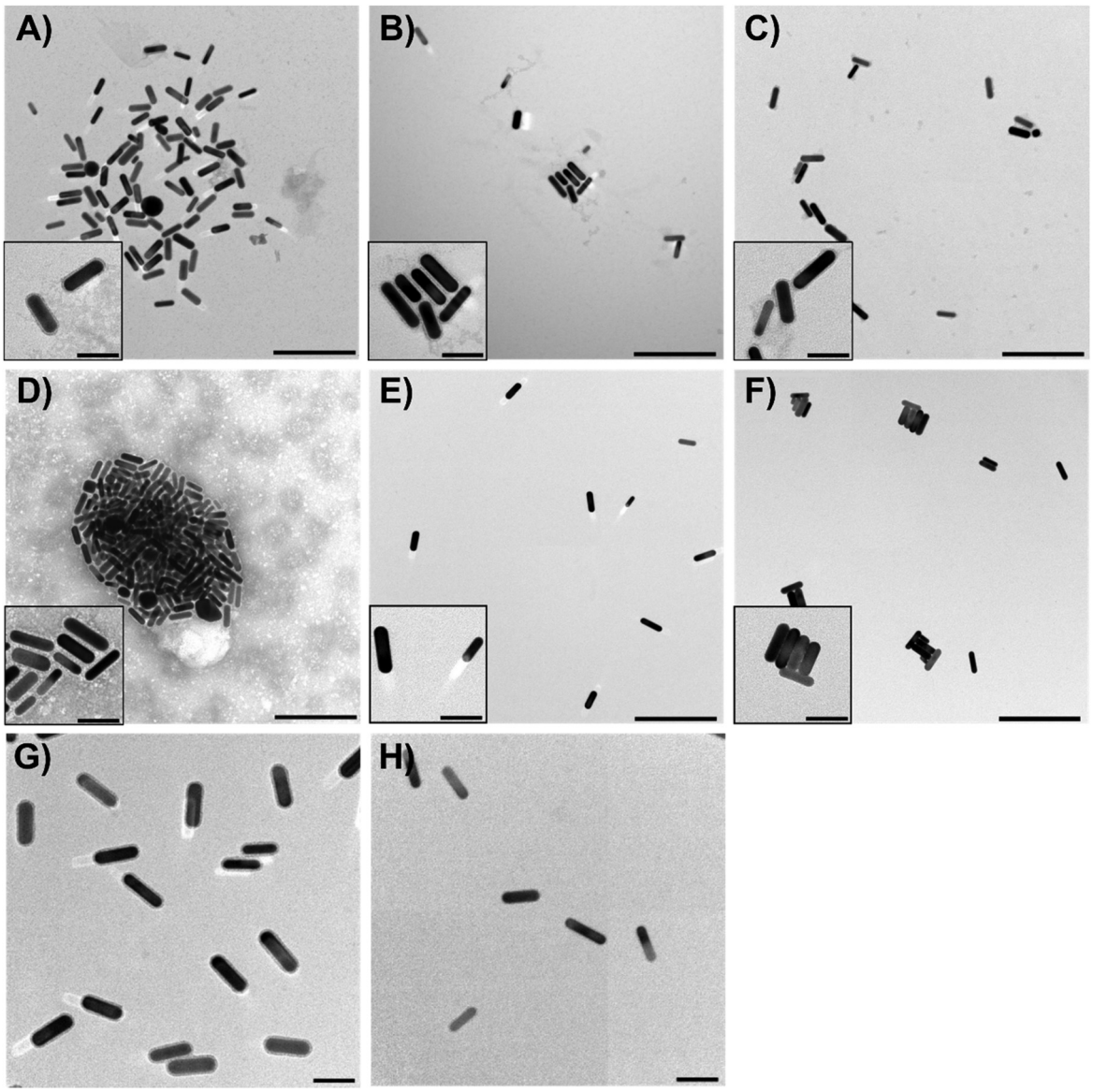

Fig. 2 Representative TEM images of GNRs coated with: (A) 1; (B) 2; (C) 3; (D) 4; (E) PEG5000; (F) PEG750; (G) **1-K**; (H) **2-K**. Scale bars: 200 nm (A–F) and 50 nm (G and H and the inserts). Samples were stained with 0.5% uranyl acetate. For low magnification images, see Fig. S11–S14 (ESI†).

of GNRs also resulted in a negative value of −15.3 mV for **GNR@PEG5000**. These changes in surface charge revealed the successful surface modification of the GNRs. However, as **1-K** and **2-K** are positively charged, both showed positive zeta-potential values (+23.6 mV for **GNR@1-K**, +18.7 mV for **GNR@2-K**), although these were somewhat lower than for **GNR@CTAB**. However, TEM imaging showed the presence of shells around these GNRs, which indicated ligand exchange had indeed occurred. Combined, these UV-Vis and TEM data show that PAs can be used to stabilise GNRs, although peptides, such as **4**, cannot.

PA-coated GNR behaviour at different ionic strengths

For PA-stabilised GNRs to be employed successfully *in vitro* and *in vivo*, they have to remain well dispersed at physiologically relevant ionic strengths. To investigate whether PA-coated GNRs were capable of this, their aggregation tendency was probed at varying sodium chloride (NaCl) concentrations. NaCl induces GNR aggregation by screening surface charges, resulting in the nanoparticles reaching their isoelectric point.[31,36] As a result, interparticle electrostatic repulsion is minimised, and the nanoparticles aggregate and precipitate from suspension. In this assay, aggregation behaviour was monitored with UV-Vis spectroscopy. A decrease in the optical density at the maximum LSPR wavelength (OD_{LSPR}) relative to the OD_{LSPR} of the sample in 0 mM NaCl indicated aggregation (Fig. S16, ESI†). Severe aggregation was considered to occur if the value of this normalized OD_{LSPR} was below 0.5.

GNRs coated with the single chain PAs **1** and **2** showed rapid (*i.e.* within 15 min) aggregation when the NaCl concentration was increased from 150 to 500 mM, while GNRs coated with the double-chain PA **3** were insensitive to high (3 M) NaCl

concentrations (Fig. 3A). PEGylated GNRs did not exhibit severe aggregation, but a 10–15% decrease in absorbance relative to 0 M NaCl indicated that PEGylated GNRs are more sensitive to charge screening than **GNR@3**. Interestingly, the zeta-potential values were similar for all three PA-coated and therefore cannot be used as a predictor of colloidal stability in this case. A possible explanation for this behaviour may be attributed to the charge distribution within the shell. This distribution, in turn, depends on the peptide chain conformation (*i.e.* its secondary structure), which can be influenced by alkyl chain parameters (*i.e.* number of chains and their length).[41]

It should be noted, that upon removal of NaCl (by means of centrifugation) the PA-stabilised GNRs regained their non-aggregated state, which means that the observed aggregation was reversible and should therefore be considered agglomeration.

Interestingly, aggregation was already observed at 50 mM NaCl with positively charged GNRs (Fig. 3B). This finding indicated these GNRs are much less stable in buffers than the GNRs coated with negatively charged PAs. Furthermore, these data imply that **GNR@1-K** and **GNR@2-K** would not be stable in biological media, where the salt concentration is higher than 50 mM. This observation is in line with previous reports regarding peptidic stabilisation of spherical GNPs: Levy *et al.* reported that negatively charged amino acid residues should be present at the opposing terminus to the GNR-binding Cys residue in order to provide enough electrostatic repulsion in 150 mM NaCl.[42] Positively charged residues placed in this position failed to stabilise the GNPs.

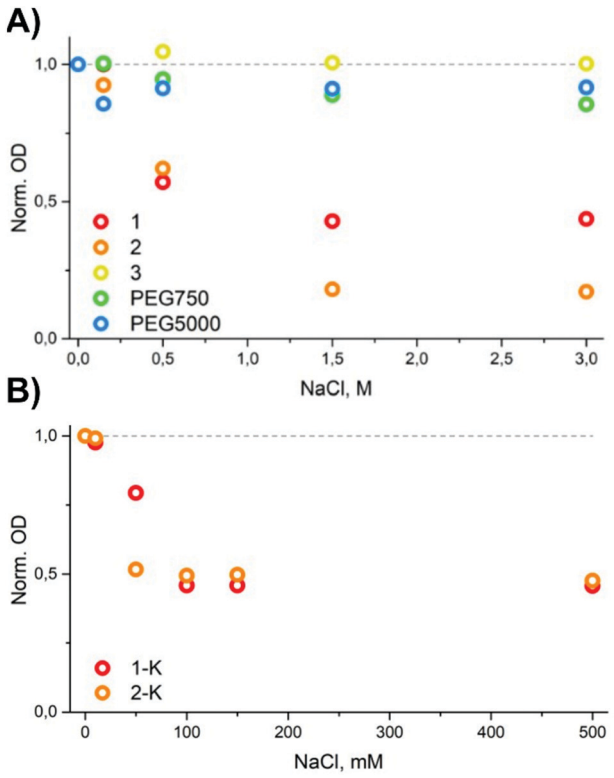

Fig. 3 Stability of PA-coated GNRs in the presence of NaCl was evaluated through the change in OD of the suspension: with increasing NaCl concentration, differing extents of GNR aggregation were observed for (A) GNRs coated with negatively-charged PAs or PEG, and (B) GNRs coated with positively-charged PAs.

We can conclude that PAs **1–3** are effective coating ligands resulting in well-dispersed single GNRs in PBS. Longer PEG molecules, such as thio-PEG (5 kDa), can also be used to effectively stabilise these GNRs, however its contour length exceeds that of PAs by 25 nm (5 nm *versus* ≈30 nm). Moreover, the shorter PEG750 had a lower stabilising capacity, as demonstrated by the small aggregates observed with TEM. **1-K** and **2-K** failed to provide sufficient stability to GNRs at biologically relevant NaCl concentrations and so were excluded from further studies. Despite this, we believe that these positively charged GNRs could be useful, for example, in biosensing applications when immobilized on a flat surface to detect analytes under continuous flow.

PAs form SAMs on the GNR surface exhibiting high coverage densities and high levels of β-structure

Coverage density is an important parameter in defining a ligand's stabilising capacity.[20] A difference in coverage density provided by **1–3** could potentially explain the difference in the behaviour of the corresponding GNRs at elevated salt concentrations. The coverage density of the bound PAs was therefore determined by UV-Vis spectroscopy.[31] To facilitate this, all three PA sequences were extended with a tryptophan (Trp, W) yielding **1-W**, **2-W**, and **3-W** (structures shown in Fig. S10, ESI†). GNRs were subsequently coated with these PAs using the same procedure as described above, except that 1,1,1,3,3,3-hexafluoro-2-propanol (HFIP) was used as the solvent instead of DMSO. HFIP exhibits a strong tendency to disrupt hydrogen bonds and was therefore deemed to provide better recovery of unbound PAs by means of centrifugation.[31] The PA concentration in the supernatants was determined and therefore the number of bound ligands could be calculated. This analysis resulted in the following coverage densities: 3.87 peptides per nm^2 for **1-W**, 3.16 peptides per nm^2 for **2-W**, and 2.62 peptides per nm^2 for **3-W**. These values are in agreement with previously reported ligand coverage densities of GNRs coated with thiolated alkyl chains analogous to the alkyl chains used in our PAs.[20,21] Moreover, the maximum theoretical coverage densities d_{theor} for **1–3** were calculated to ensure the feasibility of the observed values. Models of extended β-structured molecules **1–3** were built using PyMol and the distances between key atoms were determined (Scheme S1, ESI†). Each molecule was simplified to a geometric shape and the volume of this shape was calculated. The length of a fully-stretched molecule was taken as the shell thickness, and using the diameter of a rod (14.0 nm), the volume of the shell was calculated (Table S1, ESI†). After dividing the volume of the shell by the volume of a molecule, the following d_{theor} values were determined: 4.89 peptide per nm^2 for **1**, 4.54 peptide per nm^2 for **2** and 3.84 peptide per nm^2 for **3**. These values represent a situation when the molecules are tightly packed on the gold surface with almost no free volume within the shell. These values serve as a reference, and provide a theoretical upper limit of what

coverage is achievable. The fact that the observed coverage densities are close to these theoretical figures indicates that densely-packed self-assembled monolayers (SAMs) are formed by PAs on the GNR surface.

These calculated coverage densities increased in the order **GNR@3** < **GNR@2** < **GNR@1**. This order was explained on the basis of the PA geometry. Shortening the alkyl chain from C16 to C11 results in the peptide domain being closer to the gold surface. The steric bulk of the sidechains was therefore altered in proportion to the alkyl chain length, causing increased steric hindrance and resulting in a lower coverage density for **GNR@2** in comparison to **GNR@1**. Due to the bidentate nature of **3**, a lower peptide coverage was also expected.

Next, the secondary structure of the bound PAs was investigated. The PAs were designed to be β-structured, and it was previously shown that β-structured peptides confer higher GNP stability, due to their ability to form tight, well-packed coatings on the GNP surface.[31,42–44] Therefore, we considered it important to probe the amount of secondary structure present in the PAs that coated the GNRs.

Attenuated total reflection IR (ATR-IR) spectra of the coated GNRs were recorded to investigate the peptide secondary structure of the PAs on the GNR surface (Fig. S17, ESI†). The Amide I peak (1575–1725 cm^{-1}) reflects the conformation of the peptide backbone and is a superposition of signals caused by different secondary structure types.[45,46] An absorption band centred between 1613–1637 cm^{-1} is attributed to β-structures, a band located between 1637–1645 cm^{-1} shows the presence of unordered structures, while a band at 1645–1662 cm^{-1} is indicative of α-structures, and a band around 1662–1682 cm^{-1} reveals the presence of turns and other structures.[45–47] The Amide I region of the recorded spectra were fitted to give a sum of these four bands (Fig. 4A–C).

When the PAs were bound to the GNR surface, all three coatings were dominantly β-structured: 58.8% for **GNR@1**, 51.8% for **GNR@2**, and 57.1% for **GNR@3** (Table 1). The tendency to adopt unordered structures was low (<7%), although a significant percentage of α- and other structures were observed. The small differences in observed secondary structure types are likely to be caused by packing defects that could be linked to PA composition. For instance, molecules **2** and **3** possess a shorter alkyl chain and show a higher α-content in comparison to molecule **1**, which has a longer alkyl chain. The fact that a high proportion of β-content is observed indicates the peptidic portions of these PAs were able to effectively hydrogen bond and form well-ordered SAMs on the surface of the GNRs. These SAMs help to stabilise the GNRs, likely in a similar manner to that previously demonstrated for spherical GNPs.[31]

To further investigate the ligand organisation on the gold surface a dithiothreitol (DTT) ligand displacement assay was employed.[31] This assay probes the accessibility of the gold surface and the stability of the Au–S bond: if ligands are displaced by DTT, GNRs aggregate. This potential for displacement is important to investigate as there are molecules, such as glutathione, which are found in cells and are capable of competing

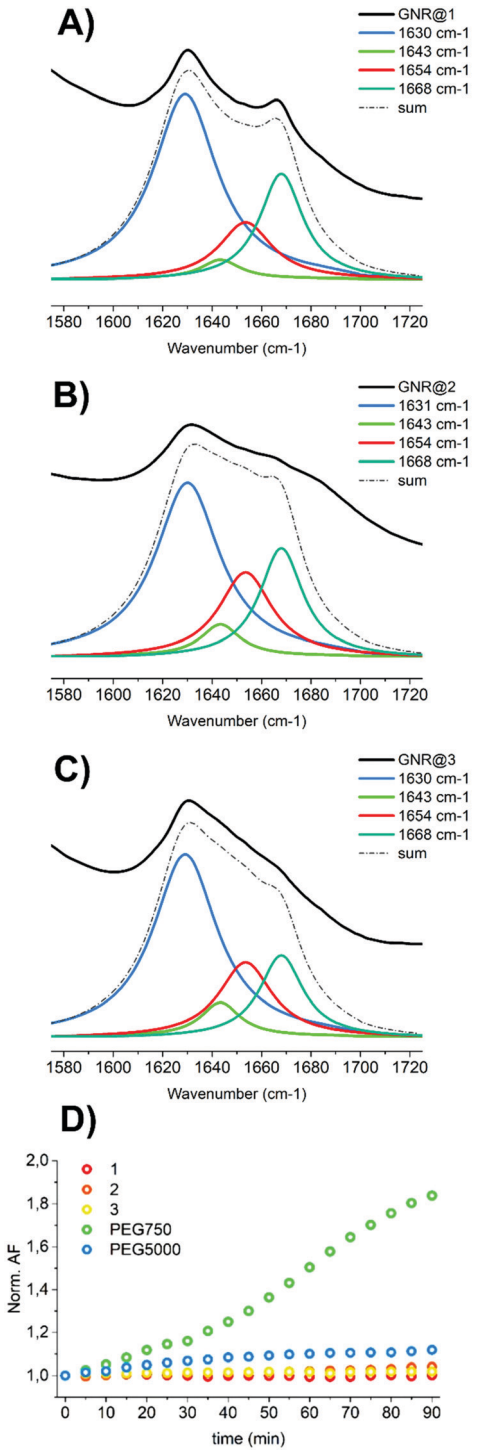

Fig. 4 Self-assembly of PAs on the GNR surface was studied using (A–C) ATR-IR for the evaluation of the peptide secondary structure and (D) a DTT assay to determine accessibility of the gold surface for competing thiols. In the ATR-IR spectra Amide I peaks were fitted as a sum of four peaks corresponding to different secondary structure types (blue line – β-structures, green line – unordered structures, red line – α-structures, cyan line – turns) for the following coatings: (A) **1**; (B) **2**; and (C) **3**. GNR aggregation in the presence of a competing thiol DTT (1 M) indicates poor self-assembly behaviour of the bound ligand or/and instability of the Au–S bond. Aggregation state of coated GNRs was monitored with UV-Vis spectroscopy and expressed by means of normalised AF (for a description of this parameter, see Fig. S18A, ESI†).

Table 1 Secondary structure distribution of PAs **1–3** bound to the GNR surface

Sample	β (%)	Unordered (%)	α (%)	Others (%)
GNR@1	58.8	3.9	14.8	22.5
GNR@2	51.8	6.0	20.5	21.7
GNR@3	57.1	6.8	19.0	17.1

The distribution is based on fitting the amide I peak with four individual peaks and is shown as a percentage. Fitting to the Lorenz function was performed using Origin Pro.

with the PAs for binding to the GNR surface. For this assay, coated GNRs were exposed to 1 M DTT and a UV-Vis spectrum was recorded every 5 min for a period of 90 min (Fig. 4D and Fig. S18, ESI†). The aggregation factor (AF)[31,36] was calculated as the ratio between the optical density at 610 nm (OD_{610}), a peak indicative of aggregation, and the OD_{LSPR}. This value is then normalised to the initial value, AF_0.

From the normalised AF plot it was obvious that all three thiolated PAs protected and insulated the GNR surface, presumably by forming an impenetrable monolayer. This was attributed to the high coverage densities provided by the alkyl chains, as well as to the presence of the hydrophobic environment they created. Water and dissolved molecules, such as DTT, cannot penetrate this hydrophobic barrier and are therefore depleted at the gold surface. In contrast, the colloidal stability of PEGylated GNRs was shown to be strongly correlated to the molecular weight of the PEG. While **GNR@PEG750** aggregated rapidly, **GNR@PEG5000** did not exhibit signs of aggregation. GNR stabilisation with PEG is based on a steric stabilisation effect: the long polymer chain wraps around the surface providing good coverage and shielding. As a result, longer PEGs provide better coverage of the gold surface.[15]

Two-photon imaging of PA-coated GNRs in zebrafish embryos.

As **GNR@3** proved to be the most stable coating for the GNRs, these particles were selected for a proof-of-principle *in vivo* imaging experiment. Before testing these particles *in vivo*, their cytotoxicity was evaluated with an LDH release assay in murine bone-marrow derived dendritic cells. These cells are known to process foreign nanoparticles entering an organism and are commonly used to study GNP behaviour.[48–50] It was found that they did not induce acute cytotoxicity when administered in a sub-nM concentration range (Fig. S19, ESI†). Similar results were reported for PEGylated GNRs.[51]

Two-photon (2P) luminescence microscopy allows for effective GNR detection, as the excitation wavelength can be matched to the LSPR of the rods. Since the LSPR of GNRs is located in the near-infrared region, this excitation wavelength means that damage to live tissue is minimized, and deep tissue imaging is possible.[5,6]

Here, the transparent zebrafish embryo (*Danio rerio*) was used as an animal model to visualise and further study PA-stabilised GNRs. The zebrafish embryo has demonstrated great potential in the screening and optimisation of nanoparticles;[52] allowing for an understanding of their *in vivo* behaviour and the identification of important nano–bio interactions of various assembled delivery systems.[53,54] **GNR@3** were intravenously injected into the duct of Cuvier of zebrafish embryos and subsequently imaged using 2P microscopy (Fig. 5 and Video S1, ESI†). It was observed that, 1.5 hours post injection, **GNR@3** remained partially in circulation (Video S1, ESI†), and some of the **GNR@3** accumulated in the caudal region of the zebrafish embryo (Fig. 5). This region consists of scavenging endothelial cells (SECs) delineating the blood vessels, that functionally resemble liver sinusoidal endothelial cells, as they express scavenger receptors such as Stabilin-1 and Stabilin-2. In addition, these receptors are known to interact and endocytose anionic nanoparticles from circulation.[39,40,55] Since **GNR@3** have a negatively charged surface, it is most likely that, mechanistically, they are interacting with SECs *via* Stabilin receptors (green arrows in Fig. 5B). Moreover, **GNR@3** interacts with apparent blood-resident macrophages, based on shape and size, (orange arrows in Fig. 5B), as previously observed.[39]

GNR@3 exhibits *in vivo* behaviour expected of nanoparticles of their size and surface chemistry: cellular uptake primarily by

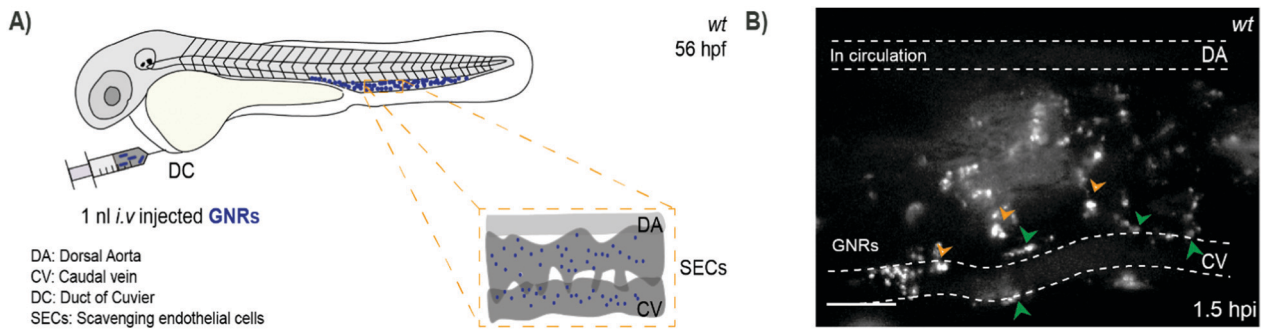

Fig. 5 Two-photon imaging of **GNR@3** *in vivo*: (A) schematic showing the site of microinjection in a zebrafish embryo at 54–56 hours post fertilization (hpf), imaged with 2P microscopy at 1.5 hours post injection (hpi). Volume of injection: 1 nL of coated GNRs (0.33 nM, PBS pH 7.2). The caudal region of the zebrafish embryo where the dorsal aorta (DA), the caudal vein (CV), and the scavenging endothelial cells (SECs) are located as depicted in the boxed region. (B) GNRs are accumulating in SECs expressing Stabilin receptors (delineating the blood vessels), indicated by green arrows, or by blood-resident macrophages (apparent macrophages containing GNRs, based on shape) indicated by orange arrows. Scale bar: 25 μm. For the transmission image, see Fig. S20 (ESI†).

SECs, partial circulation after ~1 hpi, and clearance by blood-resident macrophages as has been previously observed for negatively charged nanoparticles of different chemistries.[39,40] This demonstrates that PA-coated GNRs have the potential to act as a platform for a variety of biomedical applications (*i.e.* plasmonic photothermal therapy of cancer, GNR-mediated 2P imaging of biological targets or processes, as well as labeling, or biosensing). In addition, they are highly stable, exhibit no evidence of acute toxicity, and are easily detectable in *in vivo* systems as this proof-of-principle experiment shows. For further development of this concept, the peptide shell offers a facile route for modification with ligands of interest. This way, PA-stabilised GNRs can be endowed with targeting ligands or bioactive moieties.

Conclusions

Thiolated PAs were evaluated for their ability to form a protective coating on the surface of GNRs. Whilst both negatively charged PAs **1–3** and positively charged **1-K** and **2-K** were capable of stabilising GNRs, only the negatively charged PA-coated GNRs were stable under physiologically relevant conditions. In addition, these PAs provide greater stability compared to thiolated PEG molecules of the same contour length.

The stabilising effect of the PAs was attributed to the presence of the alkyl chain and to the formation of a self-assembled monolayer (SAM) at the GNR surface. PAs with a single alkyl chain (**1** and **2**) showed higher coverage densities that **3**, which comprised a double chain, whilst all three PAs exhibited significant amounts of β-structure (>50% content). All three PA coatings showed good stability to DTT. This was attributed to the alkyl chains present at the interface, restricting access of this water-soluble thiol to the gold surface. PA **3** was considered to be the best stabiliser for GNRs as it remained stable at extreme NaCl and DTT concentrations. Moreover, it was observed that **GNR@3** outperformed GNRs coated with thio-PEG (5 kDa) as **GNR@3** was completely insensitive to surface charge screening, and did not dissociate from the GNR surface upon addition of a competing thiol, whereas the PEG coating did show some aggregation in both assays. The superior stability of **3** is attributed to the two alkyl tails providing increased hydrophobic bulk. This bidentate nature is also beneficial because such coordination has previously been proven to provide more stable nanoparticle coatings when compared to monodentate counterparts.[36]

Furthermore, we demonstrated that **GNR@3** can be successfully visualised using 2P luminescence microscopy *in vivo*, in real time, revealing its cellular interactions and opening up opportunities for further *in vivo* studies.

Conflicts of interest

The authors declare no competing financial interests.

Acknowledgements

E. E. acknowledges the financial support of the Global Education Scholarship Program (Russia). A. K. acknowledges the support of an NWO (Netherlands Organization for Scientific Research) VICI grant (grant number: 724.014.001). R. C. V. and J. v. N. acknowledge the support of an NWO VICI grant (grant number: 680-47-616).

References

1 S. E. Lohse and C. J. Murphy, *Chem. Mater.*, 2013, **25**, 1250–1261.
2 S. Link, C. Burda, M. B. Mohamed, B. Nikoobakht and M. A. El-Sayed, *J. Phys. Chem. A*, 1999, **103**, 1165–1170.
3 B. Nikoobakht and M. A. El-Sayed, *Chem. Mater.*, 2003, **15**, 1957–1962.
4 G. González-Rubio, V. Kumar, P. Llombart, P. Díaz-Núñez, E. Bladt, T. Altantzis, S. Bals, O. Peña-Rodríguez, E. G. Noya, L. G. MacDowell, A. Guerrero-Martínez and L. M. Liz-Marzán, *ACS Nano*, 2019, **13**, 4424–4435.
5 H. Wang, T. B. Huff, D. A. Zweifel, W. He, P. S. Low, A. Wei and J.-X. Cheng, *Proc. Natl. Acad. Sci. U. S. A.*, 2005, **102**, 15752–15756.
6 N. J. Durr, T. Larson, D. K. Smith, B. A. Korgel, K. Sokolov and A. Ben-Yakar, *Nano Lett.*, 2007, **7**, 941–945.
7 L. Tong, Q. Wei, A. Wei and J.-X. Cheng, *Photochem. Photobiol.*, 2009, **85**, 21–32.
8 W. Zhang, M. Caldarola, X. Lu and M. Orrit, *ACS Photonics*, 2018, **5**, 2960–2968.
9 B. van den Broek, B. Ashcroft, T. H. Oosterkamp and J. van Noort, *Nano Lett.*, 2013, **13**, 980–986.
10 M. R. K. Ali, Y. Wu, Y. Tang, H. Xiao, K. Chen, T. Han, N. Fang, R. Wu and M. A. El-Sayed, *Proc. Natl. Acad. Sci. U. S. A.*, 2017, **114**(28), E5655–E5663.
11 G. M. Proshkina, E. I. Shramova, M. V. Shilova, I. V. Zelepukin, V. O. Shipunova, A. V. Ryabova, S. M. Deyev and A. B. Kotlyar, *Cancers*, 2021, **13**, e5235.
12 A. M. Alkilany, P. K. Nagaria, C. R. Hexel, T. J. Shaw, C. J. Murphy and M. D. Wyatt, *Small*, 2009, **5**, 701–708.
13 L. Scarabelli, A. Sánchez-Iglesias, J. Pérez-Juste and L. M. Liz-Marzán, *J. Phys. Chem. Lett.*, 2015, **6**, 4270–4279.
14 X. Ye, Y. Gao, J. Chen, D. C. Reifsnyder, C. Zheng and C. B. Murray, *Nano Lett.*, 2013, **13**, 2163–2171.
15 N. Bogliotti, B. Oberleitner, A. Di-Cicco, F. Schmidt, J.-C. Florent and V. Semetey, *J. Colloid Interface Sci.*, 2011, **357**, 75–81.
16 F. Schulz, W. Friedrich, K. Hoppe, T. Vossmeyer, H. Weller and H. Lange, *Nanoscale*, 2016, **8**, 7296–7308.
17 N. D. Burrows, W. Lin, J. G. Hinman, J. M. Dennison, A. M. Vartanian, N. S. Abadeer, E. M. Grzincic, L. M. Jacob, J. Li and C. J. Murphy, *Langmuir*, 2016, **32**, 9905–9921.
18 J. Wan, J.-H. Wang, T. Liu, Z. Xie, X.-F. Yu and W. Li, *Sci. Rep.*, 2015, **5**, e11398.
19 C. Hanske, M. N. Sanz-Ortiz and L. M. Liz-Marzán, *Adv. Mater.*, 2018, **30**, e1707003.

20 B. E. Janicek, J. G. Hinman, J. J. Hinman, S. Bae, M. Wu, J. Turner, H.-H. Chang, E. Park, R. Lawless, K. S. Suslick, C. J. Murphy and P. Y. Huang, *Nano Lett.*, 2019, **19**, 6308–6314.
21 M. Wu, A. M. Vartanian, G. Chong, A. K. Pandiakumar, R. J. Hamers, R. Hernandez and C. J. Murphy, *J. Am. Chem. Soc.*, 2019, **141**, 4316–4327.
22 R. Pardehkhorram, F. Alshawawreh, V. R. Gonçales, N. A. Lee, R. D. Tilley and J. J. Gooding, *Anal. Chem.*, 2021, **93**, 12954–12965.
23 T. Staniszewska, M. Szkulmowski and S. Morawiec, *J. Phys. Chem. C*, 2021, **125**, 14765–14777.
24 P. M. R. Paulo, P. Zijlstra, M. Orrit, E. Garcia-Fernandez, T. C. S. Pace, A. S. Viana and S. M. B. Costa, *Langmuir*, 2017, **33**, 6503–6510.
25 X. Tong, Z. Wang, X. Sun, J. Song, O. Jacobson, G. Niu, D. O. Kiesewetter and X. Chen, *Theranostics*, 2016, **6**, 2039–2051.
26 K. C. L. Black, Y. Wang, H. P. Luehmann, X. Cai, W. Xing, B. Pang, Y. Zhao, C. S. Cutler, L. V. Wang, Y. Liu and Y. Xia, *ACS Nano*, 2014, **8**, 4385–4394.
27 H. Yang, H. He, Z. Tong, H. Xia, Z. Mao and C. Gao, *J. Colloid Interface Sci.*, 2020, **565**, 186–196.
28 Z. Ma, D. N. LeBard, S. M. Loverde, K. A. Sharp, M. L. Klein, D. E. Discher and T. H. Finkel, *PLoS One*, 2014, **9**, e112292.
29 S. M. Sedlak, M. S. Bauer, C. Kluger, L. C. Schendel, L. F. Milles, D. A. Pippig and H. E. Gaub, *PLoS One*, 2017, **12**, e0188722.
30 N. S. Abadeer, M. R. Brennan, W. L. Wilson and C. J. Murphy, *ACS Nano*, 2014, **8**, 8392–8406.
31 E. A. Egorova, M. M. J. van Rijt, N. Sommerdijk, G. S. Gooris, J. A. Bouwstra, A. L. Boyle and A. Kros, *ACS Nano*, 2020, **14**, 5874–5886.
32 J. K. Sahoo, A. S. Braegelman and M. J. Webber, *J. Indian Inst. Sci.*, 2018, **98**, 69–79.
33 K. Shiraishi and M. Yokoyama, *Sci. Technol. Adv. Mater.*, 2019, **20**, 324–336.
34 C. J. Orendorff and C. J. Murphy, *J. Phys. Chem. B*, 2006, **110**, 3990–3994.
35 D. J. Mikolajczak, J. L. Heier, B. Schade and B. Koksch, *Biomacromolecules*, 2017, **18**, 3557–3562.
36 B. C. Mei, E. Oh, K. Susumu, D. Farrell, T. J. Mountziaris and H. Mattoussi, *Langmuir*, 2009, **25**, 10604–10611.
37 P. Aleström, L. D'Angelo, P. J. Midtlyng, D. F. Schorderet, S. Schulte-Merker, F. Sohm and S. Warner, *Lab. Anim.*, 2020, **54**, 213–224.
38 B. M. Weinstein, D. L. Stemple, W. Driever and M. C. Fishman, *Nat. Med.*, 1995, **1**, 1143–1147.
39 G. Arias-Alpizar, L. Kong, R. C. Vlieg, A. Rabe, P. Papadopoulou, M. S. Meijer, S. Bonnet, S. Vogel, J. van Noort, A. Kros and F. Campbell, *Nat. Commun.*, 2020, **11**, e3638.
40 G. Arias-Alpizar, J. Bussmann and F. Campbell, *Bio-Protoc.*, 2021, **11**, e4173.
41 E. A. Egorova, G. S. Gooris, P. Luther, J. A. Bouwstra, A. Kros and A. L. Boyle, *Pept. Sci.*, 2021, **113**, e24236.
42 R. Lévy, N. T. K. Thanh, R. C. Doty, I. Hussain, R. J. Nichols, D. J. Schiffrin, M. Brust and D. G. Fernig, *J. Am. Chem. Soc.*, 2004, **126**, 10076–10084.
43 C. P. Shaw, D. A. Middleton, M. Volk and R. Lévy, *ACS Nano*, 2012, **6**, 1416–1426.
44 E. Colangelo, Q. Chen, A. M. Davidson, D. Paramelle, M. B. Sullivan, M. Volk and R. Lévy, *Langmuir*, 2017, **33**, 438–449.
45 H. Susi and D. M. Byler, D. M. [13] Resolution-Enhanced Fourier Transform Infrared Spectroscopy of Enzymes, *Methods Enzymol.*, 1986, 290–311.
46 Yu. N. Chirgadze and N. A. Nevskaya, *Biopolymers*, 1976, **15**, 607–625.
47 J. Kong and S. Yu, *Acta Biochim. Biophys. Sin.*, 2007, **39**, 549–559.
48 A. Y. Lin, J. Lunsford, A. S. Bear, J. K. Young, P. Eckels, L. Luo, A. E. Foster and R. A. Drezek, *Nanoscale Res. Lett.*, 2013, **8**, e72.
49 N. Climent, I. García, M. Marradi, F. Chiodo, L. Miralles, M. J. Maleno, J. M. Gatell, F. García, S. Penadés and M. Plana, *Nanomedicine*, 2018, **14**, 339–351.
50 C. L. Villiers, H. Freitas, R. Couderc, M.-B. Villiers and P. N. Marche, *J. Nanopart. Res.*, 2010, **12**, 55–60.
51 M. Bhamidipati and L. Fabris, *Bioconjugate Chem.*, 2017, **28**, 449–460.
52 S. Sieber, P. Grossen, J. Bussmann, F. Campbell, A. Kros, D. Witzigmann and J. Huwyler, *Adv. Drug Delivery Rev.*, 2019, **151–152**, 152–168.
53 V. Saez Talens, G. Arias-Alpizar, D. M. M. Makurat, J. Davis, J. Bussmann, A. Kros and R. E. Kieltyka, *Biomacromolecules*, 2020, **21**, 1060–1068.
54 F. Campbell, F. L. Bos, S. Sieber, G. Arias-Alpizar, B. E. Koch, J. Huwyler, A. Kros and J. Bussmann, *ACS Nano*, 2018, **12**, 2138–2150.
55 G. Arias-Alpizar, B. Koch, N. M. Hamelmann, M. A. Neustrup, J. M. J. Paulusse, W. Jiskoot, A. Kros and J. Bussmann, *Nanomedicine*, 2021, **34**, e102395.

